Sequences of ground states and classification of frustration in odd-numbered antiferromagnetic rings

Wojciech Florek* and Michał Antkowiak
Faculty of Physics, Adam Mickiewicz University, ul. Umultowska 85, 61-614 Poznań, Poland

Grzegorz Kamieniarz
Faculty of Physics, A. Mickiewicz University, ul. Umultowska 85, 61-614 Poznań, Poland
and Max Planck Institute for the Physics of Complex Systems, 01187 Dresden, Germany
(Received 14 September 2016; revised manuscript received 25 November 2016; published 20 December 2016)

The sequences of ground states in frustrated antiferromagnetic rings with odd number of local spins characterized by a single bond defect or by arbitrary uniform couplings to an additional spin located at the center are determined. The sequences provide firm constraints on the total ground-state quantum numbers, which are more stringent than those arising from the Lieb-Mattis theorem for bipartite quantum spin systems. Apart from their theoretical importance, they suggest the possibility of tailoring a given class of the molecular nanomagnets with desired ground-state properties by tuning the relevant couplings. In particular, they predict the spin $S = 1/2$ ground state for the centered rings composed of the half-integer spins with approximately uniform interactions. They confirm the applicability of the recent classification of spin frustration in both types of molecular nanomagnets. The classification is also discussed in the classical limit for the first class of the rings, providing a direct picture of frustration types. The Lieb-Mattis energy-level ordering and an analog of the Landé band, i.e., the energy spectra properties simplifying the characterization of the rings using the bulk magnetic or NMR measurements, are briefly discussed.

DOI: 10.1103/PhysRevB.94.224421

I. INTRODUCTION

Synthesis of magnetic molecules has influenced both experimental and theoretical physics and chemistry, providing a variety of examples of frustrated quantum spin systems [1–7], in particular a wide class of chromium-based rings [8–12] or complexes of iron and gadolinium ions represented by centered wheels [3,13]. Their schemata corresponding to the odd-numbered rings are shown in Fig. 1. One aspect of their study is connected with envisaged practical applications in data storage and quantum computing or low-temperature cooling [13–18]. The second aspect touches on fundamentals of the theory of quantum spin systems.

The molecules can be rigorously analyzed by bulk techniques, providing test beds for the consequences of such concepts as tunneling of the magnetization, frustration, information processing, entanglement [8], or basic theorems describing the properties of the low-energy states [19]. Among the molecules intensively studied at present are the members of the Cr_8 family [8] such us the Cr_7M rings (M = Ni, Cd, Mn) [20] or their derivatives Cr_9 [9,10,21] as well as those with the Gd_7 [13] or Mn_5 [22] cores. The common feature of these molecular nanomagnets is the strong localization of the spin magnetic moment on the metallic centers which substantiates the spin model description.

Following Toulouse and coworkers [23,24] and Kirkpatrick [25], the *geometric frustration* means that in a given system there exists at least one cycle with an odd number of antiferromagnetic bonds. This criterion is fulfilled for both types of rings depicted in Fig. 1. The geometric frustration affects the ground-state energy (GS) which becomes higher than the sum of the simultaneously minimized local interactions [26,27].

Here we handle frustration following the geometric context defined by Toulouse. We note that Kahn [28] restricted the notion of frustration in molecular nanomagnets to the particular cases when the ground state is formed by the eigenstates of the corresponding spin model Hamiltonian which are accidentally degenerated for two spin quantum numbers S, at least one of them different from zero. If this condition is fulfilled, frustration is referred to as the *degenerate frustration* and this perspective is sometimes adopted in literature [9,21,29].

A need for classification of spin frustration in molecular nanomagnets was realized when the nonanuclear chromium-based rings were synthesized and analyzed [9]. In these systems it was found that the ground-state total spin S survives in a certain range after a geometric frustration is switched on and the bipartiteness of the rings is broken. To discriminate this region of frustration from that changing the GS quantum number S, the former was assigned to the third type of frustration and the latter was assigned to the second type. The first type of frustration was reserved to the Kahn degenerate frustration. This classification was then renewed and qualified [10,19].

The molecular nanomagnets exhibit their quantum properties at a very low-temperature region so that a crucial aspect of their exploration is the understanding of the low-energy spectra and the corresponding eigenstates. A step in this direction has been accomplished for the rings with a single bond defect [19], unveiling the universal GS sequence and compliance of the so-called Lieb-Mattis level ordering (LMLO). In this paper we address these problems in more detail and we include centered rings explicitly in our analysis. We start from the in-depth discussion of bipartiteness in finite systems defined by Lieb and Mattis and its consequences arising from the

*Wojciech.Florek@amu.edu.pl

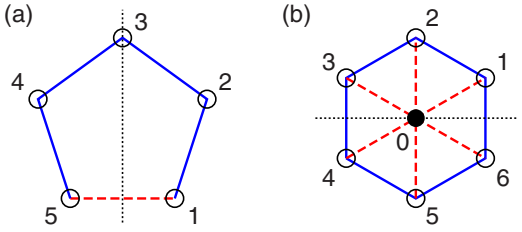

FIG. 1. Examples of the rings with odd number of quantum spins and the nearest-neighbor interactions J: (a) a regular pentagon with one bond modified and (b) a centered regular hexagon. Solid lines represent antiferromagnetic couplings with $J = 1$, whereas dashed ones correspond to those with an arbitrary value $J = \alpha$. The reflection symmetry considered is depicted by dotted lines.

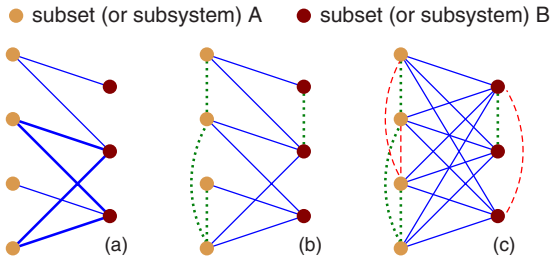

FIG. 2. (a) Bipartiteness defined in graph theory and in the Lieb-Mattis formulation (b) for $g^2 = 0$ and (c) for $g^2 > 0$. Blue (solid) lines denote graph edges or antiferromagnetic couplings with $J_{jk} \geqslant g^2$, green (dotted) lines correspond to ferromagnetic ones ($J_{jk} < 0$), and red (dashed) lines indicate antiferromagnetic couplings with $0 < J_{jk} \leqslant g^2$.

Lieb-Mattis theorem (LMT) [30–32]. Then we demonstrate the relations between bipartiteness and frustration as well as a number of results for the odd-numbered rings with either a single defected bond or with a single spin located in the center which are exemplified in Figs. 1(a) and 1(b), respectively. We also note the similarities and differences of the quantum spin systems with the Ising and classical counterparts in the case of the rings subject to a single bond defect.

II. BIPARTITENESS AND CLASSIFICATION OF FRUSTRATION IN SPIN SYSTEMS

In the Lieb and Mattis (LM) formulation [30,31] the finite spin system described by the Heisenberg Hamiltonian

$$H = \sum_{1 \leqslant j < k \leqslant n} J_{jk} \boldsymbol{s}_j \cdot \boldsymbol{s}_k \tag{1}$$

is subject to the LMT provided that it is *bipartite*. A system of *quantum* spins $\{\boldsymbol{s}_j\}$ $(j = 1,2,\ldots,n)$ is *bipartite* if a set of indices $\{1 \leqslant j \leqslant n\}$ can be decomposed into *disjoint* parts A and B, and there exists such a real number g^2 that all exchange couplings satisfy the following inequalities:

$$J_{jk} \geqslant g^2 \quad \text{for} \quad j \in A, k \in B, \tag{2a}$$

$$J_{jk} \leqslant g^2 \quad \text{for} \quad j,k \in A \quad \text{or} \quad j,k \in B, \tag{2b}$$

where the positive values are assigned to the antiferromagnetic interactions.

Then, introducing the maximum total spins in subsystems $S_A = \sum_{j \in A} s_j$, $S_B = \sum_{k \in B} s_k$ and their absolute difference

$$\mathcal{S} = |S_A - S_B|, \tag{3}$$

the LMT implies that for any g^2 and for all $S \geqslant \mathcal{S}$ the following rule is obeyed:

$$E_{\min}(S+1) > E_{\min}(S), \tag{4}$$

where $E_{\min}(S)$ denotes the minimum energy in the band corresponding to a given total spin quantum number S. This rule is referred to as the LMLO [19,33], whereas $E_{\min}(S)$ describes the so-called Landé band [2,34–37].

The value $\mathcal{S}$ given by Eq. (3) is the crucial quantity. The LMT predicts that for any bipartite system the value $\mathcal{S}$ constitutes the *upper limit* for the total spin number S in the GS, i.e.,

$$S \leqslant \mathcal{S}. \tag{5}$$

Moreover, the firm constraint (5) becomes even more stringent and implies the unique GS value $S_0 = \mathcal{S}$ in two special cases: (i) $g^2 = 0$; (ii) $\mathcal{S} \leqslant 1/2$, preserving the LMLO condition (4) for $S \geqslant S_0$. We emphasize that LMT does not hash out the validity of LMLO in the domain $S < \mathcal{S}$ and then a minimum in the Landé band may occur for $S = \mathcal{S}$.

The LM definition of bipartiteness is more general than that used in the conventional graph theory. Within the mathematical approach [38], the compact graph is *bipartite* if a set of vertexes can be decomposed into two disjoint sets A and B, and all the graph edges connect vertexes from *different* subsets only, as illustrated in Fig. 2(a). Such a bipartite graph contains only cycles with an *even* number of edges [38]. If this graph represents a system with antiferromagnetic interactions only, then it is unfrustrated. A four-edge cycle appears in Fig. 2(a) and is distinguished from the remaining edges by bold lines.

A bipartite system of quantum spins with $g = 0$ can be obtained from the bipartite graph in Fig. 2(a) when its edges represent *antiferromagnetic* interactions. In addition, the ferromagnetic couplings within the subsystems are admissible. The resulting exemplary graph of this class is shown in Fig. 2(b), where the antiferromagnetic and ferromagnetic interactions are represented by solid blue lines and dotted green lines, respectively. In the mathematical sense, these new "ferromagnetic" graph edges get a different color [39].

Interestingly, in the graphs representing a bipartite spin system with $g = 0$, only the cycles with an *even* number of antiferromagnetic interactions occur. Therefore, the *geometric* frustration is excluded in this case [23,24,29,40] and the total spin S is uniquely determined in the GS, i.e., $S_0 = \mathcal{S}$.

The LMT assumptions expressed by the inequalities in Eqs. (2) allow antiferromagnetic interactions within subsystems, but then each pair of sites belonging to different subsystems needs to be antiferromagnetically coupled with the strength which is not weaker that any antiferromagnetic coupling existing within subsystems. An example of such bipartite model system with $g^2 > 0$ is presented in Fig. 2(c), where dashed (red) lines represent intersubsystem antiferromagnetic couplings with the upper limit g^2 $(0 < J_{jk} \leqslant g^2)$.

In this type of bipartite systems, two features should be emphasized: (i) they exhibit some cycles with an *odd* number of antiferromagnetic couplings, so that they are geometrically frustrated; (ii) their GS total spin S obeys the constraint (5) despite frustration. These remarkable features were outlined for the triangular systems in the preceding publication [19] and explain why the third type of frustration may exist.

III. FRUSTRATED RINGS

The frustration in both types of antiferromagnetic rings is discussed, considering the isotropic Heisenberg models for quantum spin systems presented in Fig. 1, i.e.,

$$H_1 = \sum_{j=1}^{n-1} \boldsymbol{s}_j \cdot \boldsymbol{s}_{j+1} + \alpha \boldsymbol{s}_n \cdot \boldsymbol{s}_1, \tag{6}$$

$$H_2 = \sum_{j=1}^{n} \boldsymbol{s}_j \cdot \boldsymbol{s}_{j+1} + \alpha \boldsymbol{s}_0 \cdot \sum_{j=1}^{n} \boldsymbol{s}_j, \quad n+1 \equiv 1, \tag{7}$$

where n is an odd or even integer for H_1 and H_2, so that the odd number of sites in the ring N is equal to n or $n+1$, respectively. The local site-independent spin values s_j are arbitrary, i.e., $s_j = s$.

Due to the spherical symmetry both the total spin S and its projection M are good quantum numbers. The models are symmetric with respect to reflection ρ in the plane perpendicular to the defected bond or to an edge of the regular polygon representing the centered rings (see Fig. 1). This symmetry leads to the additional quantum number $r = \pm 1$ ($\pm$ for short) which distinguishes the *symmetric* and the *antisymmetric* states, respectively.

In the rings with a single bond defect α, the geometric frustration occurs for $\alpha > 0$, whereas in the second class considered, it is present for any $\alpha \neq 0$. From the point of view of bipartiteness of the systems (6) and (7) with arbitrary odd number N, this property is fulfilled for the first class of rings if $\alpha \leqslant 0$ with $g^2 = 0$ and for the second class, if $\alpha \geqslant 1$ with $1 \leqslant g^2 \leqslant \alpha$. However, there are notable exceptions and bipartiteness is more common in some architectures. The triangle with a single defect is bipartite with $g^2 > 0$ for arbitrary $\alpha > 0$ [19], which leads to the constraint on the total GS spin $S \leqslant s$. Moreover, in the limit $n = 2$ in Eq. (7), the centered rings can be depicted as the isosceles triangles [see Figs. 3 and 1(b)]. Their legs correspond to the identical defected bonds α and their base corresponds to the double peripheral bond. These triangles are also bipartite for $\alpha > 0$ with $g^2 > 0$, so the upper limit for their GS quantum number S amounts to s.

A. Rings with a single bond defect

In the GS, the rings of this class have the unique total spin $S = s$ for $\alpha \leqslant 0$, whereas for $\alpha > 0$ the value S is subject to the constraint $S \leqslant s$ [19]. Except for the Kahn frustration points, their energy structure is characterized by LMLO, irrespective of the bond strength α, and the allowed GS quantum numbers S forge the universal sequence in the domain $\alpha \geqslant 0$ of the

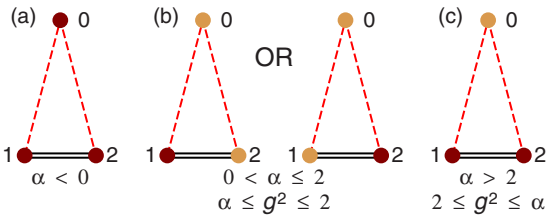

FIG. 3. Isosceles triangles representing the centered rings with $n = 2$ and their partitioning. The legs represent the defects of the strength α and the double lines in the base visualize the contribution from the first term in Eq. (7). Spins denoted by dark and light circles belong to different subsystems. The triangle in panel (a) is not bipartite, whereas those in panel (b) and (c) are bipartite.

form

$$S = s, s-1, \ldots, \left\{ \begin{array}{c} 2,1,0,1,2, \\ 3/2,1/2,1/2,3/2, \end{array} \right\} \ldots, s-1, s, \tag{8}$$

where the upper (lower) row corresponds to the integer (half-integer) spin number s, respectively. The sequence of GS's begins with $|s,+\rangle$ and ends with $|S,r\rangle$, where $r = (-1)^{2s}$. When α increases the total spin S changes according to Eq. (8), whereas the quantum number r alternates. The sequences of the quantum numbers S calculated for a regular heptagon ($n = 7$) with $s = 2$ and $5/2$ are illustrated in Fig. 4.

Hence, there are $2s+1$ different GS's separated by $2s$ Kahn frustration points characterized by the enhanced degeneracy arising from the energy-level crossings of the states with different symmetry and the quantum numbers S (except for $S = 1/2$). Thus the phenomenon of degenerate frustration is not so rare as anticipated earlier [9]. The coordinates of the corresponding level crossings $\alpha_c^{(j)}$ ($1 \leqslant j \leqslant 2s$) are exemplified in Table I (after Supplemental Material in Ref. [19]).

The value $\alpha_c^{(1)}$ terminates the domain of the GS spin $S = s$ which starts from $\alpha = 0$ and is adjacent to the unfrustrated domain $\alpha < 0$ with the same ground state. Thus the left edge of the sequence (8) is attributed to the third type of frustration [9]. We deem that the right edge of the sequence (8), which commences at $\alpha_c^{(2s)}$, represents the third type of frustration, too. In the limit $\alpha \to \infty$ the ring with an odd number n of spins can be reduced to the unfrustrated ring with $n-1$ spins and a single $s = 0$ impurity which is equivalent to the open

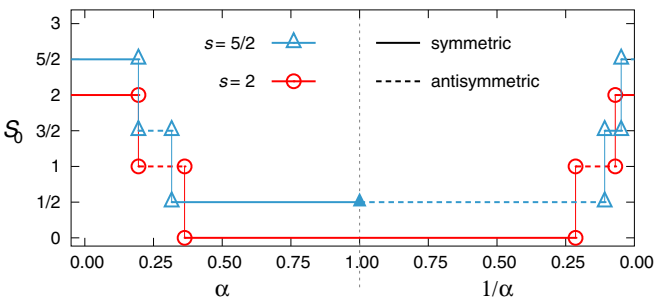

FIG. 4. The total spin S in the GS as a function of α for $n = 7$ in the cases $s = 2$ and $5/2$. For the half-integer spin $s = 5/2$ and $\alpha = 1$ the symmetry of the state $S = 1/2$ is changed; this point is denoted by a full triangle.

TABLE I. The coordinates of the consecutive level crossing points $\alpha_c^{(j)}$ for a number of spin values s and sizes n calculated for the model with a single bond defect. For half-integer spins the coordinates $\alpha_c^{(s+1/2)} = 1$ and are omitted. The results for $n = 3$ are exact.

s	j	$n = 3$	$n = 5$	$n = 7$	$n = 9$	$n = 11$
1	1	1/2	0.294	0.197	0.138	0.098
	2	2	3.562	5.438	7.777	10.790
3/2	1	1/2	0.287	0.201	0.15362	
	3	5/2	5.580	9.223	13.069	
2	1	1/2	0.279	0.195		
	2	2/3	0.470	0.363		
	3	3/2	2.564	4.671		
	4	3	8.164	14.366		
5/2	1	1/2	0.275	0.192		
	2	5/8	0.410	0.316		
	4	7/4	4.002	9.247		
	5	7/2	11.333	20.805		

segment with the GS spin $S = s$. The coordinates $\alpha_c^{(1)}$ for several fixed spin values are plotted as a function of $1/n$ in Fig. 5. The systematic decline of the data suggests that the first region of the third type of frustration shrinks to zero for the macroscopic rings.

The domain of the second type of frustration exists for $s > 1/2$ and is spread over $\alpha_c^{(1)} < \alpha < \alpha_c^{(2s)}$. This segment of the α values is split into $2s - 1$ intervals with different GS's characterized by the corresponding links in the sequences defined in Eq. (8). The adjacent intervals are separated by the Kahn degenerate frustration points (see Fig. 4).

For half-integer spins the point $\alpha_c^{(s+1/2)} = 1$ locates the level crossing of the states $|1/2,\pm\rangle$, recovering the anticipated fourfold degeneracy [41]. In particular, for α slightly higher than 1 in the spin $s = 1/2$ rings the energy levels of the GS's $|1/2,\pm\rangle$ should be close, which explains qualitatively a very small gap between the two Kramers doublets observed in the heptanuclear vanadium ring [4].

For integer spins, the coordinates $\alpha_c^{(s)} < 1$ and $\alpha_c^{(s+1)} > 1$ encompassing the value $\alpha = 1$ constitute the limits for the $S = 0$ GS domain and imply the nondegenerate GS for $\alpha = 1$, which was noticed in some particular cases [28,41].

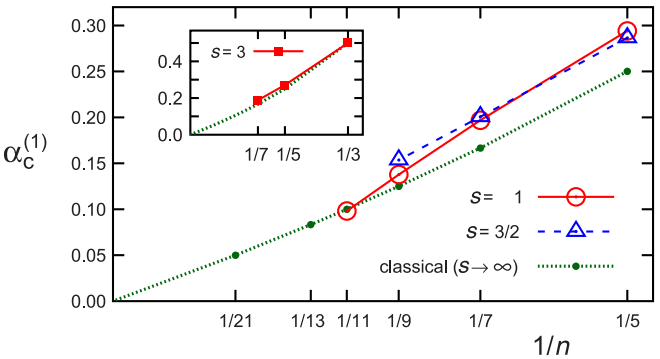

FIG. 5. The coordinates $\alpha_c^{(1)}$ as a function of $1/n$ for spin values s defined in the legend.

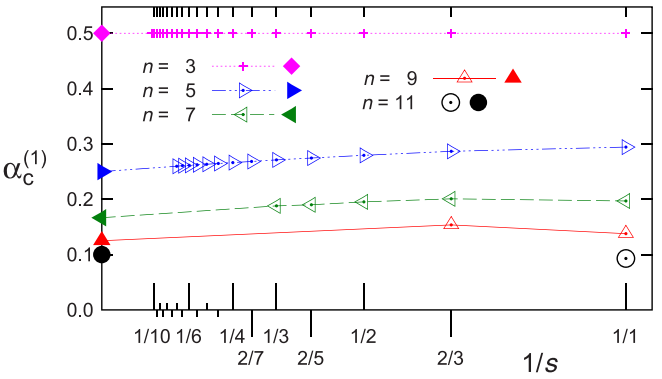

FIG. 6. Variation of the first crossing points $\alpha_c^{(1)}$ as a function of $1/s$ for a number of rings. The full symbols represent the calculated classical limits $s \to \infty$.

In Fig. 6 the variation of $\alpha_c^{(1)}$ for $3 \leqslant n \leqslant 11$ is illustrated for $s \geqslant 1$ and an evidence of the quantum effects is provided, comparing the data with respect to the classical values determined below. Recalling that for $s = 1/2$ the value $\alpha_c^{(1)} = 1$ irrespective of n, the most strong quantum effects are exposed in this case. Interestingly, the triangular structure leads to the coordination of the first Kahn frustration point $\alpha_c^{(1)}$ which coincides with the classical value $1/2$ if $s > 1/2$.

Serendipitously, all the calculations performed for nonbipartite rings indicate that LMLO given by Eq. (4) is satisfied, i.e., the differences

$$\Delta_S = E_{\min}(S) - E_{\min}(S-1) \tag{9}$$

are positive for any α except for the Kahn degenerate frustration points, where $\Delta_S = 0$. Moreover, for a fixed α the differences Δ_S form a monotonically increasing sequence. This feature implies the field-driven transitions between the ground states $M = S - 1$ and $M = S$ in the applied magnetic field [10,19].

The dependence $\Delta_S(\alpha)$ is shown for $n = 7$ and $s = 2$ in Fig. 7. As expected, for the two bottom solid lines Δ_1 and Δ_2 the dependence is not monotonic and they approach zeros at the corresponding critical values α_c listed in Table I. The four ($2s = 4$) upper curves (dotted lines) tend to linear

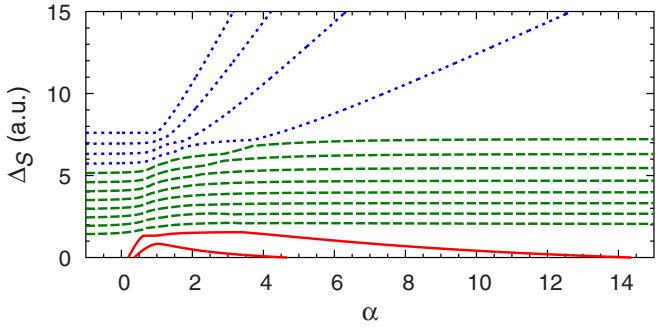

FIG. 7. The LMLO consequences in a ring with a single bond defect and $n = 7$, $s = 2$. The differences Δ_S are plotted for $1 \leqslant S \leqslant 14$ from bottom to top. Irrelevant segments are omitted. Zeros of Δ_1 and Δ_2 are placed at $\alpha = \alpha_c^{(j)}$, where $j = 2,3$ and 1,4, respectively. Different behavior for $\alpha \to \infty$ is depicted by varying line styles.

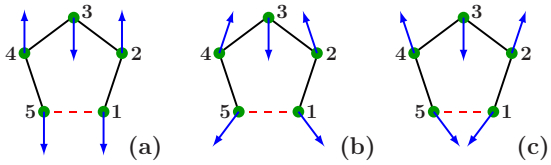

FIG. 8. The configurations corresponding to the minimum of energy for a classical antiferromagnetic pentagon: (a) $\alpha \leqslant \alpha_c$; (b) and (c) two possible configurations for $\alpha > \alpha_c$ (with different chirality); $\alpha_c = 1/4$ for $n = 5$.

functions with nonzero and increasing slopes, whereas the other $(n-3)s$ differences (dashed lines) converge to constant values. Interestingly, the ratio of the increments Δ_2/Δ_1 could be a measure of α if the first two magnetization steps were accessible experimentally.

The frustration effects can be analyzed in the classical counterpart of the model (6), considering the energy function

$$E_{\text{class}} = \sum_{j=1}^{n-1} \cos\psi_j + \alpha\cos\phi, \tag{10}$$

where $\psi_{1\leqslant j\leqslant n-1} = \angle(\vec{s}_j,\vec{s}_{j+1})$, $\phi = |\angle(\vec{s}_n,\vec{s}_1)| = |\psi_n|$, $0 \leqslant \phi \leqslant \pi$ and the length $|\vec{s}_j| = 1$. Its minima determine the stable spin configurations which yield the classical representation of the corresponding frustration types discussed. We have found that the spin vectors minimizing the function (10) are coplanar and all the angles ψ_j are the same ($\psi_j = \psi$).

In the frustration-free region $\alpha \leqslant 0$ the only configurations allowed are collinear ($\psi_j = \pi$ and $\phi = 0$), yielding the resultant vector $|\vec{S}| = |\vec{s}_j| = 1$. A possible solution for an unfrustrated pentagon (10) is shown in Fig. 8(a). The model (10) is more flexible for $\alpha > 0$ and allows both the collinear nondegenerate ($\psi_j = \pi,\phi = 0$) and noncollinear double degenerate ($\psi_j \neq \pi,\phi \neq 0$) spin configurations. They are separated by the critical value

$$\alpha_c(n) = 1/(n-1).$$

The configurations for $0 < \alpha < \alpha_c(n)$ constitute the classical representation of the third type of frustration ($|\vec{S}| = |\vec{s}_j|$). For $\alpha > \alpha_c(n)$ the first and the second types are merged. The first type is related to the twofold *chiral* degeneration observed, whereas the GS spin value criterion ($|\vec{S}| < |\vec{s}_j|$), appropriate for the second type of frustration, is also satisfied. Exemplary configurations representing the second type of frustration in a classical pentagon, which are distinguished by chirality, are presented in Figs. 8(b) and 8(c).

The sequences (8) adhere to the Ising limit of the model (6), replacing S by $|M|$, so that in the ground state $|M| \leqslant s$. The first doublet in the sequence $|M = \pm s,+\rangle$ represents GS for $\alpha < 1$. All the states of the sequence starting from $|M = \pm(s-1),-\rangle$ are degenerate and appear for $\alpha \geqslant \alpha_c = \alpha_c^{(1)} = 1$. In this way for $\alpha > 1$ the second and the third types of frustration are merged. The highly degenerated states corresponding to $\alpha > 1$ are split by the transverse spin components in the model (6), then degeneracy is lifted, bands of energy levels occur, and the full sequences (8) of GS's are formed. We emphasize that the Ising models are not classical

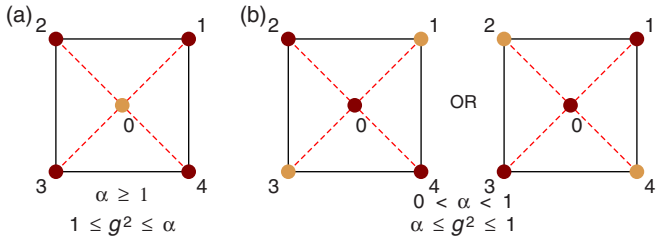

FIG. 9. A centered square representing a frustrated homogeneous spin system which for $\alpha > 0$ contains cycles $(0,j,j+1,0)$ consisting of three antiferromagnetic bonds. This system is bipartite (a) with $A = \{0\}$ when $\alpha \geqslant 1$ ($1 \leqslant g^2 \leqslant \alpha$) or (b) with $A = \{1,3\}$ when $0 < \alpha < 1$ ($\alpha \leqslant g^2 \leqslant 1$). For $\alpha < 0$ the centered square is not bipartite, whereas for $\alpha = 0$ there are two independent systems and this case is not a subject of the Lieb-Mattis theorem.

and their GS sequence resembles that of the quantum spin $s = 1/2$ models.

The Ising model satisfies the LMLO, when applied to the absolute value of the total spin component $|M|$. Since for $\alpha < 1$ the GS is characterized by $|M| = s$ and for $\alpha > 1$ it is characterized by $|M| \leqslant s$, then for all α the following inequality is satisfied:

$$E_{\min}(|M|+1) > E_{\min}(|M|) \quad \text{for} \quad |M| \geqslant s,$$

where $E_{\min}(|M|)$ denotes the energy minimum for a given $|M|$.

B. Centered rings

All the centered regular polygons with n sides are frustrated for any $\alpha \neq 0$ and bipartite for $\alpha \geqslant 1$ due to the partitioning with $A = \{0\}$ and $B = \{1,2,\ldots,n\}$, where n is even. The case $n = 4$ is exemplified in Fig. 9. Therefore, for $\alpha \geqslant 1$ the upper limit $\mathcal{S}$ of the total spin S in the GS is $\mathcal{S} = (n-1)s$ which entails the constraint

$$S \leqslant (n-1)s. \tag{11}$$

The LMLO given by Eq. (4) is automatically satisfied for the levels with the total spins $S \geqslant \mathcal{S}$.

When the coupling of the central spin is ferromagnetic ($\alpha < 0$), then the unique decomposition is $A = \{0,1,2,\ldots,n\}$ and $B = \emptyset$. This case is not excluded by the LMT [31], and leads to the trivial constraint

$$S \leqslant (n+1)s. \tag{12}$$

As in the antiferromagnetic region $0 < \alpha < 1$ the bipartiteness is violated for the rings with $n > 4$, the same result (12) could be then expected.

The constraints found are important but do not specify explicitly what are the real GS quantum numbers S and what is their dependence on α, s, or n. To address these problems, first the case $n = 4$ in the model (7) is discussed in more detail, transforming the corresponding Hamiltonian into a sublattice version [36]

$$H_2^{(n=4)} = \boldsymbol{S}_a \cdot \boldsymbol{S}_b + \alpha \boldsymbol{s}_0 \cdot (\boldsymbol{S}_a + \boldsymbol{S}_b), \tag{13}$$

where $\boldsymbol{S}_a = \boldsymbol{s}_1 + \boldsymbol{s}_3$ and $\boldsymbol{S}_b = \boldsymbol{s}_2 + \boldsymbol{s}_4$.

Its eigenvalues and eigenvectors can be obtained by the exact algebraic calculations. Skipping the technical details, the

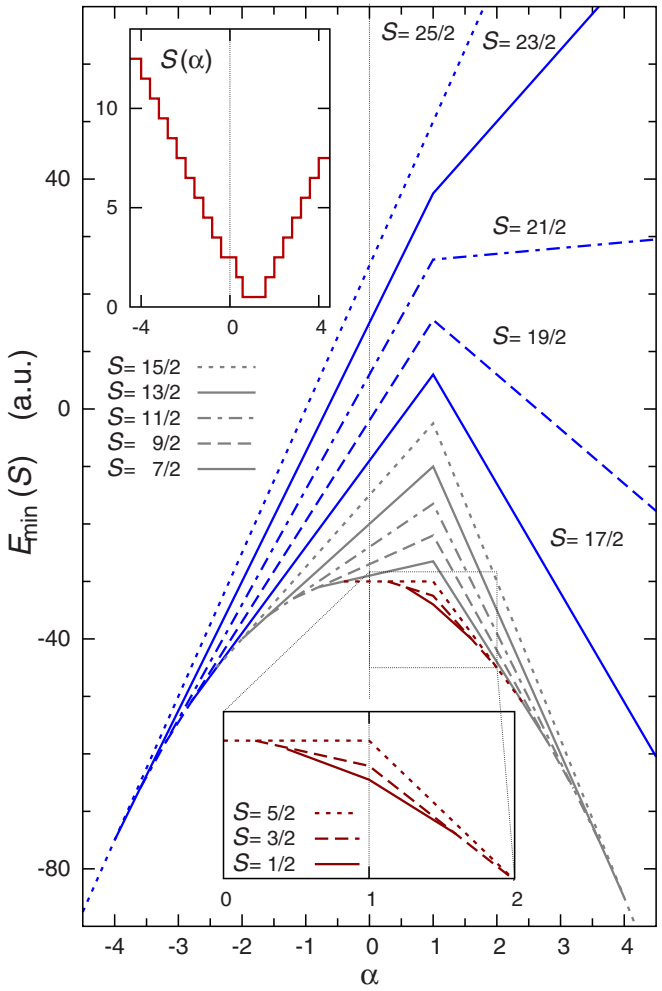

FIG. 10. The low-lying energy levels as a function of α for the centered square and $S \leqslant 25/2$. The irrelevant levels are omitted to bring out the occurrence of LMLO. In the upper inset the sequence of the allowed GS spin values S is shown for $s = 5/2$.

final results are the following. There are $8s$ critical values $\alpha_c^{(j)}$ which are spread over the interval $[-4,4]$. In the subdomain $\alpha < 0$ the critical values form the arithmetic sequence of length $4s$, where $\alpha_c^{(j)} = (j-1)/s - 4$, with $\alpha_c^{(1)} = -4$ independent of s. In the interval $0 \leqslant \alpha < 1$ the number of the critical values amounts to s or $s - 1/2$ if the spin s is integer or half integer, whereas their values are given by the expression $\alpha_c^{(4s+j)} = j/(s+1)$. Due to the bipartiteness demonstrated in Fig. 9, the LMT determines the limit $S \leqslant s$. For half-integer spins s there exists the critical value $\alpha_c^{(5s+1/2)} = 1$, where only the GS symmetry is changed with the total spin $S = 1/2$ fixed. In the remaining subdomain $\alpha > 1$, the critical values form the arithmetic sequences: $\alpha_c^{(5s+j)} = 1 + j/s$, $1 \leqslant j \leqslant 3s$, or $\alpha_c^{(5s+1/2+j)} = (2s+1)/2s + j/s$, $1 \leqslant j \leqslant 3s - 1/2$ for integer and half-integer spin numbers s, respectively. It is easy to check that the last critical value $\alpha_c^{(8s)} = 4$.

Apart from the level crossing points, the energy spectra and the eigenstates have been calculated for a variety of the spin values s. The spectra reveal the LMLO features of the model (13). In Fig. 10 the energy levels are directly plotted

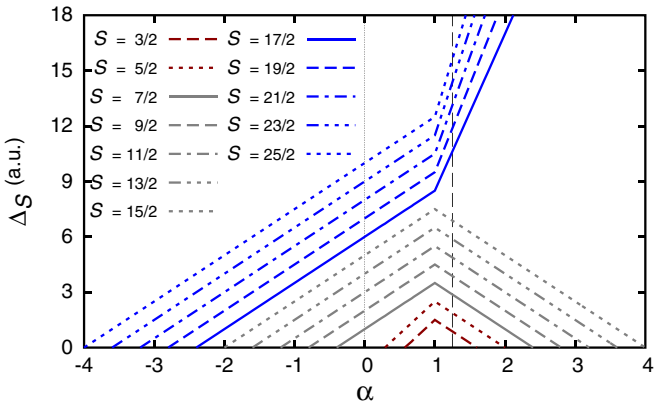

FIG. 11. The α dependence of the increments Δ_S, $S = 3/2, 5/2, \ldots, 25/2$, for the centered square and $s = 5/2$, showing the LMLO features and the prevalence of the rule $\Delta_{S+1} > \Delta_S$, $3/2 \leqslant S < 25/2$, which implies the field-driven transitions $M \to M+1$ between the ground states in the applied magnetic field. The data for $\alpha = 1.25$ (marked with the dashed vertical line) are used to plot the Zeeman diagram in Fig. 12.

as a function of α, whereas in Fig. 11 the graph illustrates the energy differences Δ_S defined in Eq. (9) which are always positive for $\alpha \neq \alpha_c^{(j)}$ as the manifestation of the LMLO and lead to an analog of the Landé band. Moreover, Δ_S forges the increasing series ($\Delta_{S+1} > \Delta_S$), what implies the regular magnetization plateaus corresponding to successive transitions $M \to M+1$ in the applied magnetic field. It is striking that an anomalous jump in the slop of the gaps Δ_S occurs in the *bipartite* region $\alpha > 1$ so that it is likely to appear also for $n > 4$. Indeed, the separation of the upper $2s$ curves seen in Fig. 11 can be also expected from the broad plateau present in Fig. 5(b) of Ref. [13] which was found for the centered hexagon.

The effect of the field-driven energy-level crossing and the abrupt change in the slope of Δ_S is shown for $\alpha = 1.25$ in Fig. 12. The ground-state energies are set to zero, so that on the horizontal axis the allowed values of M appear systematically according to the rule $\Delta M = 1$, where M is the total spin projection. The anomalous size of the magnetization step is proportional to $\Delta_{S=15/2}$ and could be a direct measure of the positive α value, if the corresponding level crossings were accessible experimentally.

Qualitatively, our results for $n = 4$ (including those for $n = 2$) can be summarized in the form of the constraints on the total spin S in the ground state:

$$s \leqslant S \leqslant (n-1)s \quad \text{for} \quad \alpha \geqslant 1, \tag{14a}$$

$$S \leqslant s \quad \text{for} \quad 0 < \alpha < 1, \tag{14b}$$

$$s \leqslant S \leqslant (n+1)s \quad \text{for} \quad \alpha < 0. \tag{14c}$$

In all the cases of α, the restrictions (14) on the spin values S are more stringent than the constraints (11) and (12) predicted from LMT, yielding the *lower bounds* for the total spin S in Eqs. (14a) and (14c), and lowering the *upper bound* in Eq. (14b).

Quantitatively, for $n = 2,4$ and the increasing parameter α, the following unique sequences of the ground-state quantum

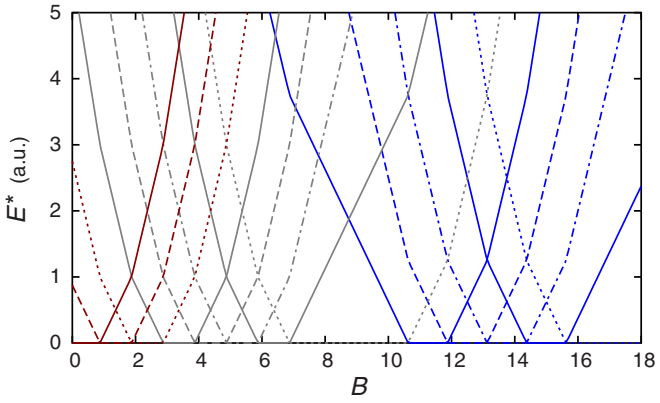

FIG. 12. The field dependence of the Zeeman energies of the $M = -S$ sublevels originating from $E_{\min}(S)$ in the dimensionless units for $s = 5/2$ and $\alpha = 1.25$, imposing $g\mu_B = 1$ and assuming that the GS energy is set to be zero $[E^*(S) = E_{\min}(S) - E_{GS}]$. As shown on the horizontal axis, the quantum numbers M change by 1, what corresponds to the height of the successive magnetization steps in the increasing magnetic field.

numbers S can be found from the algebraic calculations:

$$(n+1)s, \ldots, s+1, s, \ldots, \left\{ \begin{matrix} 1,0,1 \\ \frac{1}{2},\frac{1}{2} \end{matrix} \right\}, \ldots, (n-1)s, \qquad (15)$$

where the upper and the lower part correspond to the integer or half-integer local spin s. These sequences are universal in the sense that they are obeyed for arbitrary spin value s, but their length and the coordinates α_c of the crossing points depend on s. The corresponding sequence of the ground states begins with $|(n+1)s,+\rangle$ and terminates with $|(n-1)s,+\rangle$. The sequences in the expression (15) can be visualized as the asymmetric double staircases, as exemplified in the inset in Fig. 10 for $n = 4$ and $s = 5/2$.

We have also considered the centered rings with the size $n > 4$ and a number of spin values s by the numerical simulations within the exact diagonalization technique. We follow the convention that the number of sites in the centered ring is $N = n + 1$. The numerics reveals a picture which is coherent with the proceeding exact findings (15) for the centered square and some partial results [3]. In general, the length of the sequence (15) determining the GS total spin

TABLE II. The coordinates of the consecutive level crossing points $\alpha_c^{(j)}$ for $s = 1/2$ and some ring sizes n. The common value $\alpha_c^{(1)} = -4$ is omitted and the content is reduced due to the relation $\alpha_c^{(j)} = -\alpha_c^{(2ns+1-j)}$ for $j \leqslant ns - 1$.

j	$n = 6$	$n = 8$	$n = 10$	$n = 12$	$n = 14$
2	−3.236	−3.604	−3.759	−3.838	−3.884
3	−1.369	−2.653	−3.193	−3.466	−3.621
4	0.685	−1.045	−2.233	−2.838	−3.182
5	3.236	0.523	−0.846	−1.922	−2.541
6	4.000	2.653	0.423	−0.712	−1.685
7		3.604	2.233	0.356	−0.614
8		4.000	3.193	1.922	0.307
9			3.759	2.838	1.685

TABLE III. The coordinates of the consecutive level crossing points $\alpha_c^{(j)}$ for $1 \leqslant s \leqslant 5/2$ and some ring sizes n. The common value $\alpha_c^{(1)} = -4$ is omitted and the content is reduced due to the symmetry between $\alpha_c^{(j)}$ values.

	$n = 6$				$n = 8$	
j	$s = 1$	$s = 3/2$	$s = 2$	$s = 5/2$	$s = 1$	$s = 3/2$
2	−3.489	−3.625	−3.706	−3.758	−3.702	−3.765
3	−2.810	−3.196	−3.388	−3.504	−3.216	−3.451
4	−2.163	−2.765	−3.065	−3.246	−2.721	−3.133
5	−1.435	−2.321	−2.737	−2.985	−2.238	−2.811
6	−0.721	−1.870	−2.406	−2.722	−1.721	−2.482
7	0.360	−1.408	−2.070	−2.457	−1.147	−2.148
8	1.435	−0.940	−1.732	−2.190	−0.594	−1.810
9	2.163	−0.470	−1.389	−1.921	0.297	−1.463
10	2.810	0.282	−1.044	−1.650	1.147	−1.107
11	3.489	0.705	−0.697	−1.378	1.721	−0.743
12	4.000	1.408	−0.349	−1.104	2.238	−0.372
13		1.870	0.232	−0.829	2.721	0.223
14		2.321	0.465	−0.553	3.216	0.558
15		2.765	1.044	−0.277	3.702	1.107
16		3.196	1.389	0.198	4.000	1.463
17		3.625	1.732	0.395		1.810
18		4.000	2.070	0.691		2.148
19			2.406	1.104		2.482

values as a function of α amounts to $2ns + 1$. The consecutive values S are separated by $2ns$ Kahn level crossing points

$$-4 < \alpha_c^{(j)} < 4$$

for $1 < j < 2ns$, while $\alpha_c^{(1)} = -4$ and $\alpha_c^{(2ns)} = 4$. The values calculated for $s = 1/2$ and $6 \leqslant n \leqslant 14$ are given in Table II, whereas the remaining data for $n \geqslant 6$ are contained in Table III. We note a symmetry $\alpha_c^{(j)} = -\alpha_c^{(2ns-j+1)}$, where $1 \leqslant j \leqslant (n-1)s - 1/2$ for half-integer s or $1 \leqslant j \leqslant (n-1)s$ for integer s.

The GS sequences (15) and the coordinates of the crossing points confirm that constraints (14) are fulfilled for all the centered rings considered. Moreover, for the half-integer spins built in, there exist two neighboring states with the total spin $S = 1/2$ and different symmetry, one of them in the vicinity of $\alpha = 1$ which should be experimentally accessible. We note a numerical evidence found that the LMLO rule is satisfied for this type of rings.

The left and right edges of the GS sequences shown in Eq. (15) yield $S = (n+1)s$ and $(n-1)s$, respectively. These values coincide with those obtained for the corresponding unfrustrated rings in the limit $\alpha \to \mp\infty$. Thus according to our criterion based on the value of the GS total spin, the domains $|\alpha| > 4$ belong to the sectors of the third type of frustration.

IV. DISCUSSION AND CONCLUSIONS

The results confirm applicability of the classification of the spin frustration in molecular magnets suggested on the basis of the nonanuclear rings with a single defect and the qualitative arguments [9]. In the frustrated rings considered, there exist the ground states with the total spin S which coincides with that for the corresponding unfrustrated systems and is characteristic

for the third type of frustration. However, in the centered rings the third type of frustration is also characterized by the GS value $S = (n+1)s$ for $\alpha < -4$ and $S = (n-1)s$ for $\alpha > 4$ which correspond to those of unfrustrated rings in the proper limit. The coordinates of the GS level crossings determine the Kahn first type frustration points. Their number amounts to $2s$ and $2ns$ for the rings with a single bond defect and the centered rings, respectively, which is much higher than expected [9]. The remaining areas covered by the α values coincide with the domains of the second type of frustration.

On the basis of the algebraic calculations carried out for the small sizes N and subsequent numerical simulations performed for higher N as well as for a number of the spin variables s, the unique sequences of the GS are established. It is striking that for the rings with a single bond defect, the GS total spins S do not depend on N and are bound by the constraint $S \leqslant s$.

The chain of the allowed GS spin values is longer for the centered rings because the number of α edges amounts to $n = N - 1$. However, a half of the allowed values corresponds to the ferromagnetic coupling $\alpha < 0$ which is difficult to realize experimentally in the environment with the antiferromagnetic interactions between the peripheral spins. In practical application, we can expect that $\alpha > 0$ and then for any half-integer spins s we can expect a small value S for the moderate couplings, which can be even reduced to the GS spin $S = 1/2$ in the vicinity of the homogeneous coupling $\alpha = 1$. This feature appears irrespective of the size N and the spin value s and implies that the centered odd-numbered rings with homogeneous antiferromagnetic interactions could be considered as possible realization of the molecular qubit. This observation opens fresh scope for pursuing such spin $S = 1/2$ molecules among this type of rings. For the noncentered rings the state $S = 1/2$ is also contained in the GS sequence but for the realistic couplings in the nonanuclear chromium rings [10] the gap separating the neighboring states $S = 1/2$ and $3/2$ is too small for the practical qubit realization.

The strict compliance of the LMLO rule revealed for the rings in question is an unusual result and not expected in view of the LMT requirement of the lattice bipartiteness. For the rings with the single bond defect it was possible to refer to the bipartiteness of the isosceles triangle and speculate about the inheritance of the LMLO property. However, the isosceles triangles as building blocks of the centered rings (see Fig. 3) are not bipartite for $\alpha < 0$. It seems that the existence of the LMLO rule is a more common feature and may not be related to the bipartiteness. This supposition can be supported by the similar observation of the ordering of the lowest-energy levels with increasing S found for the spin $s = 1/2$ finite-size clusters on the triangular lattice [42]. These clusters resemble the centered rings we are dealing with and their lowest edges of the energy levels $E_{\min}(S)$ display the pure Landé-band dependence

$$E_{\min}(S) - E_{\mathrm{GS}} \sim S(S+1),$$

including the lowest value $S = 1/2$ or 0 for the clusters with the odd or even number of sites.

In the following we suggest that this behavior may not be universal but a coincidental corollary of the uniform couplings and the value $s = 1/2$. To this end, in Fig. 13 we present the energy-level diagrams calculated for the centered

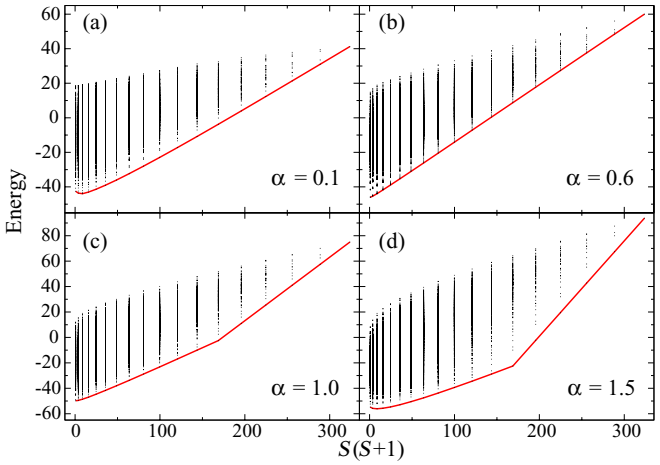

FIG. 13. The energy-level diagrams for $\alpha = 0.1$, 0.6, 1.0, and 1.5 plotted vs $S(S+1)$ in panels (a)–(d), respectively. The bottom curves depict the edges $E_{\min}(S)$.

hexagons with $s = 5/2$, assuming $\alpha = 0.6$, 1.0 for the sector corresponding to $S = 1/2$, and $\alpha = 0.1$, 1.5 for the sectors with $S = 5/2$ in the corresponding GS's. The curves visualize the dependence of the GS energies on $S(S+1)$. The straight lines comply with the Landé rule. Among the curves presented in Fig. 13, the best performance is found in the panel (b) for $\alpha = 0.6$ which yields the GS total spin $S = 1/2$. For $\alpha = 0.1$ [Fig. 13(a)] the GS spin $S = 5/2$ and, as expected, the LMLO feature $\Delta_S > 0$ is then fulfilled for $S > 5/2$, but the curve achieves the minimum for $S = 5/2$ so that clear deviations from the Landé rule appear in this part of the curve. An interesting feature is revealed for $\alpha = 1.0$ in Fig. 13(c). For this ratio the ground state is characterized by $S = 1/2$ and the first part of the curve follows through the Landé rule, but there is a cusp at the position $2s + 1$ from the end. This cusp signalizes that α is large enough to reach the area of separation illustrated in Fig. 11. The same peculiarity occurs for $\alpha = 1.5$ [Fig. 13(d)], but the minimum is exhibited for the GS spin $S = 5/2$. In relation to the clusters of $s = 1/2$ spins on the triangular lattice [42], our results suggest that the cusps expected are irrelevant. They may come out at the second to last position set out by the value $2s + 1$. However, due to the data in Table III, for the half-integer local spins $s > 1/2$ the minima in $E_{\min}(S)$ are very likely to supervene which may affect the approach applicable for $s = 1/2$ [42]. For the centered rings and $\alpha = 1.0$ (Table II) the GS spin $S = 1/2$ so that we confirm indirectly the regular Landé-like behavior observed for the finite triangle-based clusters in Ref. [42].

The LMLO implies that the nanomagnets modeled by the rings in question exhibit the magnetization plateaus with the steps of the same height corresponding to the field-induced GS transitions $\Delta M = 1$. The size of the plateaus is determined by the increments Δ_S. We note that the transitions corresponding to the field-induced level crossing can be observed also in the NMR experiments [43–45], providing the consecutive Δ_S values for $S \geqslant \mathcal{S}$.

The level crossings correspond to the Kahn degeneration points and signalize the changes in the GS spin S which determines the magnetic moment. Thus the total z component

of spin is the observable determining the ground states in the applied field, as shown in the diagram plotted in Fig. 5 in Ref. [10] and realized in some experiments [9,10,46]. Moreover, mosaics of the local magnetizations plotted therein and accessible by NMR [44] can provide indicators of the proper ground states.

These measurements are feasible on the chromium-based rings at low temperatures, as the dominant coupling is of the order of 1.4 meV and a gap to the excited states exceeds the thermal energy $k_{\mathrm{B}}T$. Thus in the Kelvin and a sub-Kelvin temperature region the phonon degrees of freedom can be neglected.

The onset of the total magnetization steps (i.e., the inflection point in the isotherms of the magnetic moment) was observed in the Cr_9 molecule with a single defected bond [10] at about $B_{\mathrm{ex}} = 4.6\,\mathrm{T} = B_{\mathrm{cr}}/2$, where B_{cr} denotes the width of the $S = 1/2$ magnetization step or $\Delta_{S=3/2}$ according to the definition (9). This value of B_{cr} implies that $\alpha \approx 0.49$, referring to the diagram in Fig. 5 in Ref. [10], which agrees very well with the value $\alpha = 0.52 \pm 0.02$ estimated independently by fitting the magnetometry data. Likewise, knowing the GS sequence (8) for $s = 3/2$, we can predict the value of α for the compound denoted by **4** in Ref. [9], which provides another example of the ring-shaped Cr_9 molecules. The fitting performed there led to the value $0.37 \lessapprox \alpha \lessapprox 0.38$. Referring to the proper magnetization curve in Fig. 2 in Ref. [9] we find $B_{\mathrm{ex}} \approx 3.7\,\mathrm{T}$ corresponding to $B_{\mathrm{cr}} = 7.5\,\mathrm{T}$. Invoking the diagram in question [10], we immediately obtain $\alpha \approx 0.38$ without any fit.

We point out that some features of the frustrated bipartite systems survive in the similar frustrated nonbipartite systems. This occurs not only for the rings considered here. For example, the Cr_8Ni molecule [46] is not bipartite but is a kind of expansion of the isosceles bipartite triangle shown in Fig. 3 with $\alpha > 1$. It is not surprising that in this case the GS sequence $2 \geqslant S \geqslant 0$ was found [47] and the corollary of the LMLO rule on the regular magnetization staircase was observed [46]. As the nonbipartite and frustrated structures are often encountered in practical realizations of the molecular rings, their interpretation within Heisenberg models would be expedited if the inheritance suggested was proved.

Finally we mention spectacular consequences of LMT applied to bipartite molecular nanomagnets. Any even-numbered ring with the nearest-neighbor antiferromagnetic interaction is bipartite with $g^2 = 0$ and yields a unique ground-state spin $S = 0$ and displays the magnetization staircase with the step heights $\Delta M = 1$ which was observed in the Fe_{10} ring with $s = 5/2$ [48]. The class of the butterfly-shape mixed valent manganese tetramers [49–51] provides another example of systems complying with the LMT assumptions. Then it is possible to predict the topology of interactions leading to the GS spin $S = 1/2$ appropriate for the molecular qubit or the high-spin value S expected for single molecule magnets if the number of half-integer spins is odd or even, respectively.

In conclusion, we have established the unique sequences of the ground states for the frustrated homometallic rings with the odd number of spins comprising either a single ($k = 1$) bond defect α or a doped spin at the center connected to all the $k = n$ peripherals by the same coupling α. The sequences are composed of $2ks + 1$ states ordered in a regular manner and constitute firm constraints on the possible total GS spin numbers S. In particular, the rings containing the half-integer spins s exhibit the ground-state spin $S = 1/2$ in the experimentally accessible range of interactions, i.e., $\alpha \simeq 1.0$.

A knowledge of the allowed ground-state quantum numbers and their relation to the relevant couplings may stimulate a search for the molecules with predictable low-temperature properties, including the molecular candidates for the quantum processing units.

The rings explored belong to a class of frustrated quantum systems preserving the Lieb-Mattis energy-level ordering which expedites their characterization by the bulk magnetic measurements or the NMR spectra. The reason for this feature is not understood for nonbipartite systems violating the LMT assumptions. Thus the molecular nanomagnets not only enable testing the concepts of quantum physics but also bring some intriguing results which are challenging for quantum theory.

The classification of spin frustration based on the ground-state total spin and its relation to the unfrustrated analog is obeyed for the rings studied. Typically the edges of the ground-state sequences belong to the domains of the third type of frustration, and the degenerate frustration occurs in the variety of the energy-level crossing points. The remaining part of the frustrated region is covered by the domain of the second type of frustration.

In the classical limit the lowest energy is reached for spin configurations which depend on α and are *symmetric* with respect to the reflection. The spin vectors are collinear for $\alpha \leqslant \alpha_{\mathrm{c}}^{(1)}(n)$ and noncollinear otherwise. Their configurations illustrate directly all the types of spin frustration in the corresponding molecular rings.

ACKNOWLEDGMENTS

This work was supported in part by the Narodowe Centrum Nauki (Poland) within Project No. N519 579138. We acknowledge access to the high-performance computing resources in Poznan Supercomputer and Networking Center Poznań (Poland) and those available within the Distributed European Computing Initiative program by the Partnership for Advanced Computing in Europe-3IP project (Seventh Framework Programme RI-312763).

[1] C. Schröder, H. Nojiri, J. Schnack, P. Hage, M. Luban, and P. Kögerler, Competing Spin Phases in Geometrically Frustrated Magnetic Molecules, Phys. Rev. Lett. **94**, 017205 (2005).

[2] L. Engelhardt, M. Luban, and C. Schröder, Finite quantum Heisenberg spin models and their approach to the classical limit, Phys. Rev. B **74**, 054413 (2006).

[3] A. M. Ako, O. Waldmann, V. Mereacre, F. Klöwer, I. J. Hewitt, C. E. Anson, H. U. Güdel, and A. K. Powell, Odd-numbered Fe^{III} complexes: Synthesis, molecular structure, reactivity, and magnetic properties, Inorg. Chem. **46**, 756 (2007).

[4] N. Hoshino, M. Nakano, H. Nojiri, W. Wernsdorfer, and H. Oshio, Templating odd numbered magnetic rings: Oxovanadium

heptagons sandwiched by β-cyclodextrins, J. Am. Chem. Soc. **131**, 15100 (2009).

[5] P. Kögerler, B. Tsukerblat, and A. Müller, Structure-related frustrated magnetism of nanosized polyoxometalates: aesthetics and properties in harmony, Dalton Trans. **39**, 21 (2010).

[6] A. N. Bilyachenko, A. I. Yalymov, A. A. Korlyukov, J. Long, J. Larionova, Y. Guari, A. V. Vologzhanina, M. A. Es'kova, E. S. Shubina, and M. M. Levitsky, Unusual penta- and hexanuclear Ni(ii)-based silsesquioxane polynuclear complexes, Dalton Trans. **45**, 7320 (2016).

[7] A. N. Bilyachenko, A. I. Yalymov, M. M. Levitsky, A. A. Korlyukov, M. A. Es'kova, J. Long, J. Larionova, Y. Guari, L. S. Shul'pina, N. S. Ikonnikov, A. L. Trigub, Y. V. Zubavichus, I. E. Golub, E. S. Shubina, and G. B. Shul'pin, First cage-like pentanuclear Co(II)-silsesquioxane, Dalton Trans. **45**, 13663 (2016).

[8] M. L. Baker, T. Guidi, S. Carretta, J. Ollivier, H. Mutka, H. U. Güdel, G. A. Timco, E. J. L. McInnes, G. Amoretti, R. E. P. Winpenny, and P. Santini, Spin dynamics of molecular nanomagnets unravelled at atomic scale by four-dimensional inelastic neutron scattering, Nat. Phys. **8**, 906 (2012).

[9] M. L. Baker, G. A. Timco, S. Piligkos, J. S. Mathiesone, H. Mutka, F. Tuna, P. Kozłowski, M. Antkowiak, T. Guidi, T. Gupta, H. Rath, R. J. Woolfson, G. Kamieniarz, R. G. Pritchard, H. Weihe, L. Cronin, G. Rajaraman, D. Collison, E. J. L. McInnes, and R. E. P. Winpenny, A classification of spin frustration in molecular magnets from a physical study of large odd-numbered-metal, odd electron rings, Proc. Natl. Acad. Sci. USA **109**, 19113 (2012).

[10] M. Antkowiak, P. Kozłowski, G. Kamieniarz, G. A. Timco, F. Tuna, and R. E. P. Winpenny, Detection of ground states in frustrated molecular rings by in-field local magnetization profiles, Phys. Rev. B **87**, 184430 (2013).

[11] O. Cador, D. Gatteschi, R. Sessoli, A.-L. Barra, G. Timco, and R. E. P. Winpenny, Spin frustration effects in an odd-member antiferromagnetic ring and the magnetic Möbius strip, J. Magn. Magn. Mater. **290–291**, 55 (2005).

[12] M. L. Baker, A. Bianchi, S. Carretta, D. Collison, R. J. Docherty, E. J. L. Mclnnes, A. McRobbie, C. A. Muryn, H. Mutka, S. Piligkos, M. Rancan, P. Santini, G. A. Timco, P. L. W. Tregenna-Piggott, F. Tuna, H. U. Güdel, and R. E. P. Winpenny, Varying spin state composition by the choice of capping ligand in a family of molecular chains: detailed analysis of magnetic properties of chromium(III) horseshoes, Dalton Trans. **40**, 2725 (2011).

[13] J. W. Sharples, D. Collison, E. J. L. McInnes, J. Schnack, E. Palacios, and M. Evangelisti, Quantum signatures of a molecular nanomagnet in direct magnetocaloric measurements, Nat. Commun. **5**, 5321 (2014).

[14] G. A. Timco, S. Carretta, F. Troiani, F. Tuna, R. J. Pitchard, C. A. Muryn, E. J. L. McInnes, A. Ghirri, A. Candini, P. Santini, G. Amoretti, M. Affornte, and R. E. P. Winpenny, Engineering the coupling between molecular spin qubits by coordination chemistry, Nat. Nano. **4**, 173 (2009).

[15] B. Georgeot and F. Mila, Chirality of Triangular Antiferromagnetic Clusters as a Qubit, Phys. Rev. Lett. **104**, 200502 (2010).

[16] F. Troiani and M. Affronte, Molecular spins for quantum information technologies, Chem. Soc. Rev. **40**, 3119 (2011).

[17] R. Sessoli, Chilling with magnetic molecules, Angew. Chem., Int. Ed. **51**, 43 (2012).

[18] R. Sessoli, Toward the quantum computer: Magnetic molecules back in the race, ACS Central Sci. **1**, 473 (2015).

[19] G. Kamieniarz, W. Florek, and M. Antkowiak, Universal sequence of ground states validating the classification of frustration in antiferromagnetic rings with a single bond defect, Phys. Rev. B **92**, 140411(R) (2015).

[20] S. Piligkos, H. Weihe, E. Bill, F. Nesse, H. E. Mkami, G. M. Smith, D. Collison, G. Rajaraman, G. A. Timco, R. E. P. Winpenny, and E. J. L. McInnes, EPR spectroscopy of a family of $Cr_7^{III}M^{II}$ (M = Cd, Zn, Mn, Ni) 'wheels': Studies of isostructural compounds with different spin ground states, Chem.—A Eur. J. **15**, 3152 (2009).

[21] E. Garlatti, S. Bordignon, S. Carretta, G. Allodi, G. Amoretti, R. De Renzi, A. Lascialfari, Y. Furukawa, G. A. Timco, R. Woolfson, R. E. P. Winpenny, and P. Santini, Relaxation dynamics in the frustrated Cr_9 antiferromagnetic ring probed by NMR, Phys. Rev. B **93**, 024424 (2016).

[22] C. Kozoni, E. Manolopoulou, M. Siczek, T. Lis, E. K. Brechin, and C. J. Milios, Polynuclear manganese amino acid complexes, Dalton Trans. **39**, 7943 (2010).

[23] G. Toulouse, Theory of the frustration effect in spin glasses: I, Commun. Phys. **2**, 115 (1977), reprinted in Ref. [26], pp. 99–103.

[24] J. Vannimenus and G. Toulouse, Theory of the frustration effect. II. Ising spins on a square lattice, J. Phys. C **10**, L537 (1977).

[25] S. Kirkpatrick, Frustration and ground-state degeneracy in spin glasses, Phys. Rev. B **16**, 4630 (1977).

[26] *Spin Glass Theory and Beyond*, edited by M. Mézard, G. Parisi, and M. A. Virasoro (World Scientific, Singapore, 1987).

[27] *Frustrated Spin Systems*, edited by H. T. Diep (World Scientific, Singapore, 2004).

[28] O. Kahn, Competing spin interactions and degenerate frustration for discrete molecular species, Chem. Phys. Lett. **265**, 109 (1997).

[29] J. Schnack, Effects of frustration on magnetic molecules: A survey from Olivier Kahn until today, Dalton Trans. **39**, 4677 (2010).

[30] E. Lieb, T. Schultz, and D. Mattis, Two soluble models of an antiferromagnetic chain, Ann. Phys. (NY) **16**, 407 (1961).

[31] E. Lieb and D. Mattis, Ordering energy levels of interacting spin systems, J. Math. Phys. **3**, 749 (1962).

[32] E. Lieb and D. Mattis, Theory of ferromagnetism and the ordering of electronic energy levels, Phys. Rev. **125**, 164 (1962).

[33] J. Richter, N. Ivanov, K. Retzlaff, and A. Voigt, Marshall-Peierls phase rule and Lieb-Mattis level ordering in non-bipartite low-dimensional antiferromagnets, J. Magn. Magn. Mater. **140–144**, 1611 (1995).

[34] J. Schnack and M. Luban, Rotational modes in molecular magnets with antiferromagnetic Heisenberg exchange, Phys. Rev. B **63**, 014418 (2000).

[35] O. Waldmann, Spin dynamics of finite antiferromagnetic Heisenberg spin rings, Phys. Rev. B **65**, 024424 (2001).

[36] W. Florek, L. A. Kaliszan, H. W. Kunert, and A. G. J. Machatine, Small antiferromagnetici spin systems—sublattice Hamiltonians, Physica B **405**, 3811 (2010).

[37] A. Furrer and O. Waldmann, Magnetic cluster excitations, Rev. Mod. Phys. **85**, 367 (2013).

[38] R. J. Wilson, *Introduction to Graph Theory*, 4th ed. (Addison-Wesley, London, 1996).

[39] The relation between frustration andgraph edges coloring was indicated, e.g., in P. Combe and H. Nencka, Frustration and overblocking on graphs, Math. Comput. Modell. **26**, 307 (1997).

[40] S. M. Giampaolo, G. Gualdi, A. Monras, and F. Illuminati, Characterizing and Quantifying Frustration in Quantum Many-Body Systems, Phys. Rev. Lett. **107**, 260602 (2011).

[41] K. Bärwinkel, P. Hage, H.-J. Schmidt, and J. Schnack, Quantum numbers for relative ground states of antiferromagnetic Heisenberg spin rings, Phys. Rev. B **68**, 054422 (2003).

[42] B. Bernu, P. Lecheminant, C. Lhuillier, and L. Pierre, Exact spectra, spin susceptibilities, and order parameter of the quantum Heisenberg antiferromagnet on the triangular lattice, Phys. Rev. B **50**, 10048 (1994).

[43] M.-H. Julien, Z. H. Jang, A. Lascialfari, F. Borsa, M. Horvatić, A. Caneschi, and D. Gatteschi, Proton NMR for Measuring Quantum Level Crossing in the Magnetic Molecular Ring Fe_{10}, Phys. Rev. Lett. **83**, 227 (1999).

[44] E. Micotti, A. Lascialfari, F. Borsa, M.-H. Julien, C. Berthier, M. Horvatić, J. van Slageren, and D. Gatteschi, Spin dynamics at the level crossing in the molecular antiferromagnetic ring $[Cr_8F_8Piv_{16}]$ from proton NMR, Phys. Rev. B **72**, 020405(R) (2005).

[45] E. Micotti, Y. Furukawa, K. Kumagai, S. Carretta, A. Lascialfari, F. Borsa, G. A. Timco, and R. E. P. Winpenny, Local Spin Moment Distribution in Antiferromagnetic Molecular Rings Probed by NMR, Phys. Rev. Lett. **97**, 267204 (2006).

[46] Y. Furukawa, K. Kiuchi, K. I. Kumagai, Y. Ajiro, Y. Narumi, M. Iwaki, K. Kindo, A. Bianchi, S. Carretta, P. Santini, F. Borsa, G. A. Timco, and R. E. P. Winpenny, Evidence of spin singlet ground state in the frustrated antiferromagnetic ring Cr_8 Ni, Phys. Rev. B **79**, 134416 (2009).

[47] M. Antkowiak, Ł. Kucharski, and G. Kamieniarz, Non-uniform coupling model of the frustrated chromium-based ring Cr_8 Ni, EPJ Web Conf. **75**, 05007 (2014).

[48] K. L. Taft, C. D. Delfs, G. C. Papaefthymiou, S. Foner, D. Gatteschi, and S. J. Lippard, [Fe(OMe)2(O2CCH2Cl)]10, a molecular ferric wheel, J. Am. Chem. Soc. **116**, 823 (1994).

[49] A.-J. Zhou, J.-L. Liu, R. Herchel, J.-D. Leng, and M.-L. Tong, High-spin tetranuclear $Mn^{II}_2Mn^{IV}_2$ clusters with unique Mn(II)–Mn(IV) magnetic exchange: synthesis, structures, and magnetism, Dalton Trans. 3182 (2009).

[50] L. B. Jerzykiewicz, J. Utko, M. Duczmal, P. Starynowicz, and P. Sobota, Tetranuclear manganese complexes with $[Mn^{II}_4]$ and $[Mn^{II}_2Mn^{III}_2]$ units: Syntheses, structures, magnetic properties, and DFT study, Eur. J. Inorg. Chem. **2010**, 4492 (2010).

[51] M. Sobocińska, M. Antkowiak, M. Wojciechowski, G. Kamieniarz, J. Utko, and T. Lis, New tetranuclear manganese clusters with $[Mn^{II}_3Mn^{III}]$ and $[Mn^{II}_2Mn^{III}_2]$ metallic cores exhibiting low and high spin ground state, Dalton Trans. **45**, 7303 (2016).